

The Analysis of Red Giant Branch Photometry in Galaxies

C. M. Frayn¹, G. F. Gilmore¹

¹ Institute of Astronomy, University of Cambridge, Cambridge, CB3 0HA, UK

Submitted to MNRAS, June 2002

ABSTRACT

We present an analysis of the many possible methods for simulating and analysing colour-magnitude diagrams, with application to studies of the field halo stellar populations of resolved galaxies. Special consideration is made to the analysis of stars on the Red Giant branch (RGB), and methods for obtaining metallicity distributions for old populations based on analysis of evolved sections of the Colour Magnitude Diagram (CMD). These tools are designed to provide a reliable and accurate method for the analysis of resolved Population II stars in the haloes of nearby galaxies.

In particular, we introduce a Perpendicular Distance method for calculating most likely source isochrones for stars in our input dataset. This method is shown to have several advantages over a more traditional approach considering the isochrone as a set of finely-spaced Gaussian probability distributions. We also consider methods by which the obtained metallicity distribution might be most efficiently optimised and especially evaluate the difficulties involved in avoiding sub-optimal local maxima in the likelihood maximisation procedure.

Key words: galaxies: haloes – stars: Population II – methods: data analysis – Hertzsprung-Russell (HR) diagram

1 INTRODUCTION

Stellar populations in galaxies encode the star formation and merger histories of galaxies, the relationship between gas in- and out-flows and the local star formation rate over time. Extensive studies of the stellar populations in the central regions of galaxies, bulges and disks, have quantified knowledge of the dominant metal-rich populations. Galaxies with substantial disks cannot have experienced recent major mergers – thus their field halo stars uniquely record their early history and minor mergers.

The stellar haloes of galaxies contain both the very oldest metal poor stars (Population II) and the debris of continuing accretion, which may have a wide range of ages and abundances. The relative importances of early formation and later accretion are a key test of hierarchical galaxy formation models, yet remain extremely poorly known.

In particular, it would be interesting to analyse nearby galaxies for comparison with current theory. Simulations of hierarchical Cold Dark Matter (CDM) cosmologies predict that massive ellipticals form at redshift < 1 (Kauffmann 1996; Baugh, Cole & Frenk 1996; Baugh et al. 1998). This may disagree with many current observational results (e.g. Daddi, Cimatti & Renzini 2000), who suggest that many large ellipticals were already in place well before this. It is

an important task, therefore, to analyse stellar populations in a robust and realistic manner.

A task of fundamental importance in this problem is determining the metallicity distribution function as this distinguishes between simple coeval populations, and those accumulated over a longer time period in a continually enriched interstellar medium. This would allow us to discriminate the roles of infall, accretion and recycling of materials on galactic time-scales. Most importantly it would allow us to distinguish between an initial burst of unenriched star formation at high redshift and later bursts triggered by the merger of gas-rich clumps of higher abundance. Do protogalaxies lose their gas before merging, or does substantial star formation still occur during the merger process in the sense proposed for globular clusters by Ashman & Zepf (1992), and observed in, for example, the Antennae galaxies by Whitmore & Schweizer (1995) and Whitmore et al. (1999)?

In this paper we discuss a set of tools developed for the analysis and interpretation of the halo stellar populations in nearby galaxies. We discuss firstly the method by which artificial stellar populations may be produced in order to compare with real datasets. In the third section, we discuss the way we can build on this work in order to fit metallicity distributions to stellar populations, given accurate photometry of their RGB populations. We explicitly include practical algorithm implementation details, and describe several

alternative approaches, as such a description is crucial to applications in astrophysics. We apply these techniques to HST data in forthcoming papers.

2 CREATING ARTIFICIAL COLOUR-MAGNITUDE DIAGRAMS

The method of stellar population synthesis has been used since the early 1980s (see eg Bruzual, 1983) primarily for the analysis of unresolved stellar populations. It was refined by Charlot & Bruzual (1991) and later by Bruzual & Charlot (1993). They proposed a new method of populating colour-magnitude space by interpolating between a large library of accurately calculated theoretical isochrones. This is the method adopted by this work, here applied to resolved populations.

The Bruzual & Charlot method relies on the fact that any stellar population can be considered as the linear sum of single stellar populations of delta-function-like distribution in age and metallicity (Z). This holds true if the spacing between these constituent functions is small enough to be insignificant compared to the observational errors.

To generate a complex stellar population, therefore, requires a simple linear sum of a set of appropriately normalised single stellar populations each generated from one single isochrone.

2.1 Isochrone selection

The isochrones used in this study are those by Girardi et al. (2000). We shall consider only V and I CMDs here, although the methods described apply equally well to any suitable choice of filters.

Uncertainties in the choice of the appropriate stellar model can result in a very different isochrone for some stages of stellar evolution. See, for example, the work done on convective overshooting by Bertelli et al. (1990) and that on alpha-enhancement by Salaris, Chieffi & Straniero (1993). Isochrone matching problems are considered in detail in our second paper (in press), together with the intrinsic systematic errors inherent in the technique of isochrone fitting. We consider here the numerical techniques required to implement the methodology.

2.2 Isochrone interpolation - the grid formalism

The first step in our method is to generate a fine grid of isochrones, with age and metallicity steps significantly smaller than the observational error. This becomes the basis for the simulated stellar population. One then generates a population distribution in age and metallicity, fixed discretely to these grid points. Each grid point corresponds to one isochrone, so that after the population has been created, populating a complex system becomes a matter of cycling through each grid point, generating a list of stellar masses using the given Initial Mass Function (IMF), the mass ranges of that particular isochrone and the relevant observability constraints.

We use the technique of automatic critical point analysis in order to interpolate accurately between adjacent isochrones (Fig. 1). This method allows us to identify the

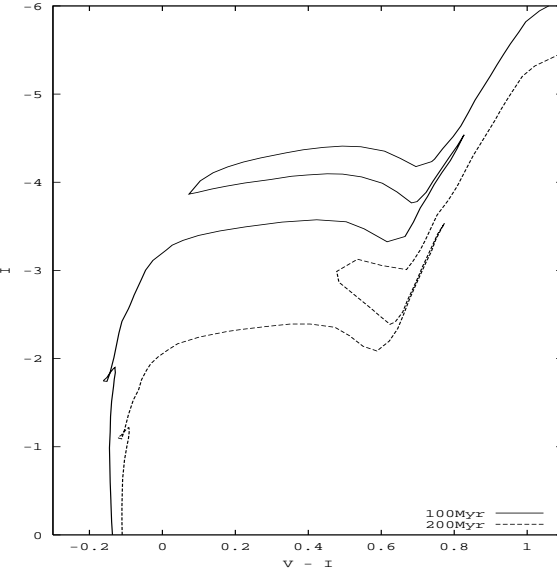


Figure 1. An example of isochrones showing sharp ‘critical turning points’. Isochrones are for 100Myr and 200Myr, with a metallicity of one-fifth solar. Isochrones from Girardi et al. (2000)

parts of the isochrones which are most important, and pair them up so that these features are carefully preserved.

Girardi et al. (2000) identify the more rapidly changing positions in their isochrone set, but in general this information is not available except by inspection. In this work we identify these points automatically by considering sharp changes in the tangent gradient to the isochrone curve. We consider here the V , $V - I$ plane, though future studies will also include other information available in the isochrone data, such as plots of $\log(L)$ vs. $\log(T_{\text{eff}})$, in which these loci are more distinct.

When the critical points have been identified, we must pair them up and then interpolate between them. At this stage it is necessary to calculate the extent to which we must interpolate between the available isochrones. This is mainly a trade off between the computational time required to interpolate the isochrones and the requirements for the accuracy of the CMD.

Clearly, if we choose a fairly coarse isochrone spacing in age and metallicity, then this limits our sampling accuracy. Correspondingly it is wasteful to store isochrones to extremely high precision in metallicity and Age. A sensible balanced medium of these two cases is required.

Once the isochrone set has been fully interpolated then we can produce artificial stellar populations using it. In our code, an input central metallicity and age is specified for each population, together with Gaussian spreads in each quantity, and the desired photometric errors, population size, completeness limit and IMF. Stars are generated according to the input distribution, and then their details are calculated by clipping them to the nearest isochrone model and reading off the desired observational properties, interpolating in mass as required.

2.3 Introducing errors

Often we require a simulation of a stellar population as it would be seen from a significant distance, for example the

halo of a nearby galaxy. In this case it is important to add in completeness effects so that the number of stars tails off to fainter absolute magnitude rather than increasing with the background correspondingly increasing.

An indication of the form of a completeness function can be derived analytically for the ideal case of isolated sources on a smooth background. For ease of calculation, and due to the low importance of the exact form of the completeness function to our methods, we decided to model this effect as a cutoff varying linearly between $\pm 1\text{mag}$ above and below the completeness magnitude. This value is either specified manually or determined experimentally by examining the luminosity function of the low-magnitude stars in the data set. The exact value of this limiting luminosity is not of great importance to the subsequent analysis.

We also introduce random photometric errors into the dataset, using a user-defined scale value set at run-time and a Gaussian smoothing kernel.

3 FITTING METALLICITY DISTRIBUTIONS TO CMD DATA

The process of obtaining star-formation histories from CMD data has produced a great deal of literature in recent years. Amongst them are reviews and analyses by Aparicio et al. (1996), Tolstoy & Saha (1996), Dolphin (1997) and Hernandez, Valls-Gabaud & Gilmore (1999).

The main important differences between all of these methods and that outlined here is the depth of the photometry involved. All four of these examples consider photometry down to the Main-Sequence Turn-Off (MSTO) magnitude. Our method was designed to be applicable mainly to the RGB stars, and is therefore optimised for fitting old, evolved populations where the age-metallicity degeneracy still causes considerable problems. We therefore cannot consider our input isochrones to represent a set of unique *eigenpopulations*, but rather a spanning, but oversampled set.

In addition, we have focused on the optimisation procedure. Most methods have adopted relatively simple methods for discovering the best-fitting model coefficients. These do not address the risk of completely missing a globally optimum solution in complex CMDs, with the exception of the method of Hernandez et al. (1999). Harris & Zaritsky (2001) consider a gradient-walker method, as outlined below, with safeguards against converging towards a local minimum. Our methods differ from theirs in three main areas. Firstly, we consider several different methods both for generating probability matrices and for optimising coefficients, testing each in turn. Secondly, we analyse the degree to which each method avoids falling into only local minima. Thirdly, we start our optimisation procedure with a first guess coefficient vector rather than a random initial guess, which goes some way to alleviating this problem.

In the following sections we discuss several methods for generating probability matrices and optimising model-fitting coefficients, and explain the advantages and disadvantages of each.

Finally, we introduce a new method for calculating the isochrone fitting coefficients for each star that leads to an accurate output metallicity determination which is robust to a real (model) dispersion.

3.1 Methods

In order to analyse any CMD data it is necessary to compare the loci of stars detected in the given CMD to the positions of theoretical isochrones. This is the principle of ‘isochrone fitting’.

There is an inbuilt complexity with isochrone fitting, namely the age-metallicity degeneracy. The effects of increasing metal abundance on stellar isochrones are remarkably similar to those of increasing age. In fact, with the absence of any other diagnostic methods, it becomes impossible to separate the two effects in some parts of the CMD, hence the degeneracy. For a population of age 2Gyr and metallicity of one half solar, doubling the metallicity has a very similar effect on the locus of the RGB as an increase in age to 7Gyr. The most important place on the isochrone where this is not true is at the MSTO.

At the MSTO, the effects of age and metallicity are different, and vary depending on the wavelength at which they are examined.

However, the MSTO is significantly below the tip of the RGB, by approximately 6 magnitudes in I for an intermediate age population, and significantly more for older populations. Clearly extremely deep images are required to achieve this kind of photometry in external galaxies, and this simply is not possible for galaxies far outside the Local Group. For the majority of targets it is therefore impossible to achieve sufficiently deep photometry to resolve the MSTO, and the degeneracy remains.

3.2 The old-age restriction.

This study deals primarily with the analysis of Population II stars in galaxy haloes. To analyse intermediate age stars we need to use different techniques. The use of the AGB can help to place restrictions on the ages of intermediate-age stars, but this is of no help for stellar populations older than 7 or 8 Gyr. At older ages, the AGB is much fainter and the main diagnostic tool we have is the RGB. Fortunately, at old age, the effects of age on the RGB are minimal, and the dominating parameter is metallicity.

Figure 2 demonstrates the difference between age and metallicity variation at high ages.

Notice how the age increase of more than 50 percent has very little effect on the colours and magnitudes of stars, whereas the metallicity increase from half-solar to solar abundances has an enormous effect. For populations of 10Gyr or older, an age variation of a few Gyr is important at approximately the same level as a metallicity variation of 0.07 dex at solar abundance. This causes a degeneracy in the metallicity distribution at approximately this level for a population with a 2Gyr age spread. For more coeval populations with narrow age spreads, the metallicity smearing effect is even lower.

Though this does not break the degeneracy per se, it certainly alleviates the problems it causes. Old RGB stars can be analysed with an assumed age, and a fairly accurate metallicity distribution can be obtained. Note that this method only applies to the RGB. By the time one reaches the horizontal branch then second parameter effects render this method useless.

Hence, the metallicity distributions that we recover us-

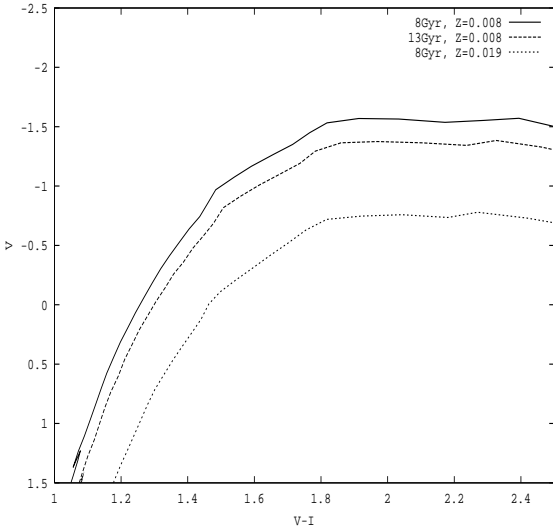


Figure 2. The difference between RGB isochrones of different ages is small at old ages. Metallicity, however, remains an important discriminator. Here we have plotted one isochrone for an 8Gyr old population with half solar metallicity (solid line). The difference caused by increasing the age by 8Gyr to 13Gyr (dashed line) is not particularly large, but that caused by increasing the metallicity to solar abundance (dotted line) is far greater.

ing our methods are only approximations to the true form, assuming one single age. For old populations, our results will be a good approximation to the metallicity distribution of the stellar population as a whole, regardless of age spread. For populations with younger components, the true metallicity values recovered should not be taken quite so literally. Instead, what we can recover is the overall *form* of the metallicity distribution, allowing us to identify the existence and relative sizes of any low- and high-metallicity components, though not their precise metallicity values.

This method for obtaining metallicity spreads is naturally dependent on obtaining photometry sufficiently deep to avoid biasing against the higher-metallicity components. Clearly from Fig. 2, photometry only complete to -1.5 in V would introduce a strong bias against higher-metallicity populations.

In addition there will be a slight bias due to the fact that populations of different metallicities evolve at slightly different speeds, so therefore we expect the size of the RGB population as a fraction of the entire population to vary with metallicity. Thus, if we have shallow photometry covering just the RGB we expect to make errors of the order of 10% in the relative weighting of metal-poor populations over metal-rich populations. This is a minor effect compared with other sources of numerical error.

4 BAYES' THEOREM & BAYESIAN INFERENCE

Bayes' theorem allows one to calculate the probabilities of certain models having created an observed data set. This probability can be maximised in order to discover the most likely model, or formation scenario for those data. Bayesian Inference is vital in determining the most probable distribu-

tion of metallicities in any stellar population. A more rigorous review of this process is found in Tolstoy & Saha (1996).

Consider a set of observed data, A , together with a set of models, B , from which we presume all of the observed data could have been derived. The problem we face is to find the most probable model, B_{best} , in a rigorous way. Essentially, which of these models, B_n , has the highest probability of producing the observed data, A ?

We introduce the nomenclature A_n being the n^{th} element of the data set A . B is defined as the set of all possible models, with each model B_n , comprising a linear combination of (non-orthogonal) basis elements.

The probability of an observed data set, A , being observed and B_n being the model which created it is simply given by;

$$P(A, B_n) = P(A|B_n) \times P(B_n) \quad (1)$$

From this, it is trivial to derive Bayes' theorem, which states;

$$P(B_n|A) = \frac{P(A|B_n) \times P(B_n)}{P(A)} \quad (2)$$

In other words, the probability of a certain model, B_n being the true model, given the observed data A , is related to the probability of obtaining those data A from model B_n and the prior probability of model B_n , together with a normalisation factor.

This normalisation factor, $P(A)$, is straightforward to calculate. In the special case where the models B_n are exclusive and exhaustive, it reduces to the following;

$$P(A) = \sum_n P(A|B_n) \times P(B_n) = C \quad (3)$$

where C is a constant. Thus we can rewrite equation (2);

$$P(B_n|A) = \frac{P(A|B_n) \times P(B_n)}{C} \quad (4)$$

$P(B_n)$ is known as the prior distribution, and allows us to bias the probabilities if we know that one particular model is *a priori* more likely than another. Essentially, if we calculate that a dataset is equally likely to have come from two separate distributions but that one of the distributions occurs more often in nature, then without any further contradictory evidence, it is safe to assume that this is the more probable distribution to have created the observed data.

In the astronomical context, we have very little prior knowledge of the metallicity distribution functions involved. Initially, it is safe to assume that all models are equally likely, though later we will introduce the concept of penalty functions, attempting to impose a certain form to the distribution function such as smoothness or a Gaussian profile.

4.1 Model fitting

We have obtained an expression telling us how we discover the most probable model given the data available. Assuming the $P(B_n)$ are all the same, as above, then we have;

$$P(B_n|A) \propto P(A|B_n) \quad (5)$$

So the problem of finding the most probable input distribution reduces initially to one of finding the distribution

which maximises the likelihood of creating the given data. Of course in reality we cannot possibly consider the totality of all possible models, as this is prohibitively large, but we can only consider a subset. It is necessary, then, to consider a sensible subset that is guaranteed to include a good approximation to the globally most likely model, and as little else as possible. Of course, *a priori* we have no idea what the most likely model is, so we consider a sensible subset of all models depending on the problem.

In this work, we wish to fit a metallicity distribution to an observed stellar population with an observational constraint that this population is ‘old’. We have already generated a large library of isochrones with which this hypothesis can be tested. The problem reduces to the following:

What linear combination of isochrones of varying metallicity and age best reproduces the distribution of stars in an input dataset?

In fact, we have considered only a subset of this question. We know that the Age-Metallicity-Distance degeneracy prohibits an absolute solution to this problem without unobtainably deep data. Instead we adopt in turn a set of single ages, initially 12Gyr, and then fit a metallicity distribution assuming each age in turn. The degree to which the stars cannot be fit using this assumption tells us a little about the degree to which the coeval assumption is incorrect. We vary the assumed age, and study the variations in the derived metallicity profile.

That is to say, we need to find the optimum set of coefficients, α_n , to maximise the product;

$$L = \prod_i \left(\sum_j \alpha_j P_{ij} \right) \quad (6)$$

where P_{ij} is the probability that star i was obtained from isochrone j . The calculation of this matrix is discussed in section 5, and the process of optimising the coefficients is discussed in section 6.

5 ISOCHROME FITTING

The first implementation problem we encounter is that of calculating the probability matrix, P_{ij} , which lists the probability of star i having come from isochrone j . Clearly we need an accurate measure of this quantity, which will allow us then to optimise the weightings for each isochrone such that the overall probability of the observed distribution coming from the given combination of isochrones is maximised.

5.1 Determining the probability matrix, P_{ij}

The fundamental part of the optimisation process is determining an accurate probability matrix, P_{ij} . To do this, we require a method of calculating whether or not one star came from a particular isochrone, based only on a discrete parameterisation of the isochrone and the observed position of the star, together with any known observational errors. Clearly for a theoretical population, the only errors are those caused by numerical problems, rounding off problems etc. However, for a real population, we need to account for the fact that

real stars do not behave optimally, and also that real detectors are not perfect. Therefore, there is a finite measurement error in both V and I .

That is, just because a star does not *appear* to lie on a particular isochrone, we cannot be sure that its displacement is not entirely caused by observational errors. Also, we must account for the fact that our isochrone models are not exact representations of observed RGBs, as discussed earlier.

5.2 Gaussian magnitude errors

It is useful to consider a set of N points arranged in a CMD at positions $\gamma_n = (\gamma_n^x, \gamma_n^y)$. Associated with each of these points is an error in each of x and y , or alternatively the magnitude and colour parameters. We could just as easily work with the two individual magnitude parameters, such as V and I , as a magnitude-magnitude diagram (MMD) contains exactly the same information as a CMD, just arranged in a different manner.

Regardless of the parameterisation, we designate each point as γ_n , and the associated errors on this measurement as $\delta_n = (\delta_n^x, \delta_n^y)$. Thus we associate a probability density distribution, $\rho(x, y)$, with every point in space. If we assume that the probability density distribution is Gaussian in form then we can assign a bivariate Gaussian probability function to ρ thus;

$$\rho(x, y) = \frac{1}{2\pi\delta_n^x\delta_n^y} \exp \left[-\frac{1}{2} \left\{ \frac{(x - \gamma_n^x)^2}{\delta_n^x} + \frac{(y - \gamma_n^y)^2}{\delta_n^y} \right\} \right] \quad (7)$$

This is normalised so that the integral over all space

$$\int \int_{-\infty}^{\infty} \rho(x, y) dx dy = 1 \quad (8)$$

If we sum over all of the points in our distribution, we obtain the total probability density at a point at position $\mathbf{r} = (\mathbf{x}, \mathbf{y})$. We designate this as $p(\mathbf{r})$;

$$p(\mathbf{r}) = \sum_i \rho_i(\mathbf{x}, \mathbf{y}) \quad (9)$$

where $\rho_i(x, y)$ is the contribution to ρ from the i^{th} point in the distribution.

We now apply this to isochrones, introducing the concept of an isochrone parametrised as a number of discrete points, rather than a continuous distribution. The more points we have, the closer this approximation becomes.

This determines the probability that any observed star came from a specified isochrone, j as P_{ij} . That is defined from equation (9);

$$P_{ij}(\mathbf{r}) = \sum_i \rho_i^j(\mathbf{x}, \mathbf{y}) \quad (10)$$

where ρ_i^j is the probability density function arising from the i^{th} star in isochrone j .

The probability that some distribution of stars arose from a certain isochrone is;

$$\xi_n = \prod_i P_{ij} \quad (11)$$

and therefore for some linear sum of isochrones, with coefficients α_j , we derive the likelihood L that some distribution of stars, labelled as i , came from the distribution of

isochrones labelled j . This is the result stated in equation (6) above.

Of course, this likelihood is only an expression of the **unnormalised** probability distribution, and we can not obtain any absolute estimate on the quality of our model fits simply from this value. However, it gives us a relative measure whereby we can compare any two distributions and assess which is a ‘better fit’ to the data.

In addition, we maximise the natural logarithm of this quantity, that is;

$$\ln L = \sum_i \ln \left(\sum_j \alpha_j P_{ij} \right) \quad (12)$$

This is bijectively related to the likelihood in the range under consideration, with no change of ordering, that is;

$$\forall \{a, b\} \in \mathbb{R}^+, a < b \Rightarrow \ln(a) < \ln(b) \quad (13)$$

So that the operation of \ln is order-preserving. This means that maximising this logarithm is equivalent to maximising the likelihood itself.

It is important that the isochrone is sufficiently finely interpolated so that the spacing between points is of the same order of the Gaussian errors, or less. This ensures that the final answer is not a strong function of the actual parameterisation of the isochrones, and is an accurate representation. In practice, it is sensible to allow interpolation of the input isochrone to arbitrary fractions of the Gaussian errors in the required colours.

The summation need be carried out only over a small subset of the total number of isochrone points in practice. This is because the value of a Gaussian probability distribution rapidly drops after a few error radii, and by the time either one of the displacements reaches 7 or 8 σ then the probability is, to all practical purposes, zero. Therefore a binary search was used to find the nearest isochrone point to the observed CMD point, and a restricted number of points in the vicinity of this one point were included in the calculation.

In this way, all the points which were capable of contributing a non-negligible fraction to the likelihood were calculated, with a minimum of extra stars outside the tolerance radius. This reduced the order of this operation from $O(n)$, where n was the isochrone length, to a constant independent of n , depending only on the level of isochrone interpolation. The binary search was extremely fast, and though it had a greater (logarithmic) time complexity, its contribution to the computation time was always negligible.

This bivariate Gaussian method has several advantages over other similar methods:

(i) The precision of this method is defined by the accuracy of the isochrone interpolation. The more accurate one requires the probabilities, the more finely one needs to interpolate the isochrone.

(ii) This method has a strong statistical grounding, building only on known properties of the error distributions involved, both those due to observational techniques, and those intrinsic to the distribution under study.

(iii) The bivariate Gaussian probability distribution is robust, if slow, to calculate.

However, it does introduce some unwanted problems:

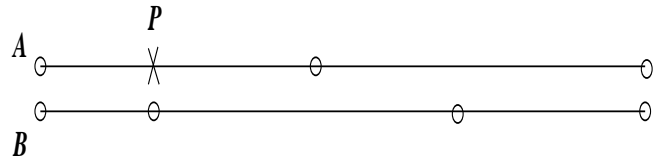


Figure 3. The problem of assigning stars to the wrong isochrone segment.

(i) Discrete parameterisation of the isochrones introduces an extra spread in probabilities due to the fact that some points will, purely by chance, fit less suitable isochrones.

(ii) Calculating a large probability matrix is rather slow, taking several minutes for a heavily populated CMD and a finely interpolated isochrone set.

(iii) Further interpolation of the isochrones is necessary, though theoretically this gives us no more information than it originally contains, thus this method is inefficient.

An illustration of the first of these problems is shown in figure 3. The point labelled P actually comes from isochrone A , but the Gaussian probability method described above would assign a larger probability of this point belonging to isochrone B , simply because of the discrete parameterisation. Of course, this problem is alleviated somewhat by a sufficiently fine isochrone interpolation.

We also investigated other methods of generating the probability matrix.

5.3 The Perpendicular Distance Method

A second method for generating the probability density matrix, P_{ij} , is the perpendicular distance method. This is potentially more accurate, though slightly more difficult to implement. The method was formulated in order to avoid the problems described above due to the discrete nature of the isochrones and the possibility of this causing misclassification problems. A method was desired which was more information-efficient than the Gaussian method described above, and also faster to calculate.

The obvious solution to the problem was to abandon the Gaussian distribution of points, and instead calculate how far any particular star is from each isochrone in a perpendicular sense. In other words, calculate the closest distance between any star and each isochrone, and assign a probability based on just these distances, rather than a sum over all isochrone points.

Actually calculating the nearest distance is simple. Some geometry gives the following relation;

$$h = \frac{2}{R} \left((x - x_1)(y_2 - y_1) - (y - y_1)(x_2 - x_1) \right) \quad (14)$$

where

$$R = \sqrt{(x_2 - x_1)^2 + (y_2 - y_1)^2} \quad (15)$$

The only real problem is how to determine the nearest two points, designated P_1 and P_2 in figure (4). Initially

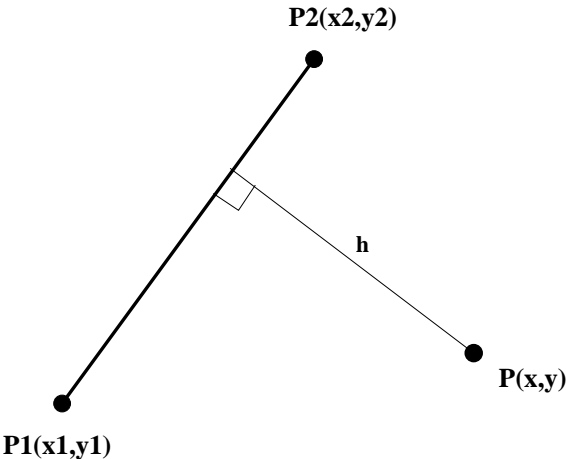


Figure 4. Geometry for the perpendicular distance value.

it seemed easiest to use the nearest isochrone point to the star under consideration, plus the nearest of its two immediate neighbours in the isochrone. In practice this led to many problems, so we decided to parse through the entire isochrone, calculating the perpendicular distance for each pair of points, and then finding the minimum value, after applying mass-weightings and cutoff-weightings (see section 5.4).

Now the perpendicular distance has been calculated, it is a simple matter of calculating the Gaussian probability density of this value. This is given by;

$$P_{ij} = ke^{-\frac{h^2}{2\sigma^2}} \quad (16)$$

Where σ is a combined error radius, and k is a constant defined to give answers in a reasonable range. Clearly, we are uninterested in the exact value of k as only relative probabilities are considered. Provided the same value of k is chosen for all calculations then the relative probability ratios will be the same regardless of the exact value chosen.

It is, of course, possible to split up the perpendicular vector into two components parallel to the colour and magnitude axes. This means that different errors in the two filters can be considered without any added difficulty simply by using a bivariate Gaussian distribution to assign the probability instead of the above method.

5.4 Mass weighting and cutoff weighting

Part of Bayes' theorem states that all models are equally likely in the absence of any prior information to the contrary. Clearly, introducing more information known to be intrinsic to the problem under study can only improve our chances of retrieving a sensible and accurate answer, provided that such information is indeed sensible and accurate.

In any stellar population, stars are produced with a certain IMF. For the RGB, most stars have the same mass to within a very small fraction. However, this paper describes a general procedure which can be applied to stars of any mass or luminosity, in principle. We therefore adopt the Kroupa, Tout & Gilmore (1993) mass function, which takes the following form;

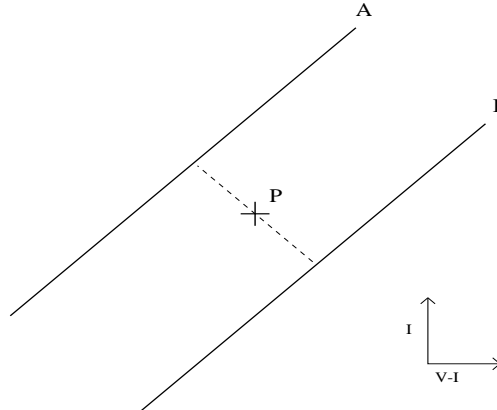


Figure 5. An illustration of how completeness effects can bias probabilities between otherwise equidistant isochrones. Here, the star is more likely to have come from the isochrone whose intersection point is at a brighter magnitude.

$$N(m) \propto m^{-\alpha} \quad (17)$$

with the following 3-element power law slope;

$$\begin{aligned} \alpha = 2.7 & \quad \text{when } m > 1.0M_{\odot} \\ \alpha = 2.2 & \quad 0.5 \leq m \leq 1.0M_{\odot} \\ 0.7 \leq \alpha \leq 1.85 & \quad 0.08 < m < 0.5M_{\odot} \end{aligned} \quad (18)$$

Taking this information, we can apply it to the calculation of the probability matrix, P_{ij} . If we have a star which is equidistant from two separate isochrones, then we can calculate the mass that this star would have at the nearest point in each isochrone, and bias the probability by this. Clearly the chances are that it came from the isochrone for which this interpolated mass is smallest.

Therefore we can bias the probability of each star coming from each isochrone by the IMF factor calculated as above in equation (18). The IMF has also to be taken into account for the normalisation in the Gaussian approach, section 5.2. However, in the Perpendicular Distance method of section 5.3 we need not do this.

We may also bias the probability by the completeness function for the point at which the perpendicular displacement touches the isochrone, or the nearest isochrone point to the star under question. Of course this is not possible with the Gaussian method, as we don't calculate the luminosity of the perpendicular intersection points.

In figure 5, the star P is equidistant from two isochrones, but the perpendicular displacement towards isochrone A touches at a brighter apparent magnitude, so we can say that this star is more likely to have come from isochrone A than isochrone B , all other effects being identical. This works only for stars around the completeness limit, of course. It is contrary to the bias introduced by the IMF.

5.5 Comparing the methods

The Perpendicular Distance method has several advantages;

- (i) Probabilities are independent of the exact position of the isochrone points, provided that the isochrone is sufficiently accurately interpolated in the first place.
- (ii) No further interpolation of the isochrone is required.

Therefore this method is optimal in terms of information efficiency.

(iii) This method is much faster than the Bivariate Gaussian sum described in section 5.2 above.

(iv) Because of the way this method treats stars lying very close to isochrones, where the perpendicular displacement is less than the average isochrone point separation, the probability gradient is much steeper than for the Gaussian method. This makes it easier to reject particularly unlikely models, especially in datasets with small photometric errors.

However, it does also have some drawbacks;

(i) This method is not as easy to enhance accurately with mass-weightings. See section 5.4 for details.

(ii) Linear interpolation has a larger effect on the errors here than it did in the Gaussian method because we are dealing with just one measurement, rather than the sum of several, and therefore a substantial fractional error could prove significant to the overall probability.

(iii) Most importantly, this method is susceptible to endpoint errors.

It is worthwhile considering the last two of these problems in turn.

5.5.1 Linear interpolation problems

In this method, the effects of linear interpolation between points are more pronounced. With the Gaussian error box method of section 5.2, we knew that at least some of the points we considered were at the correct place in the isochrone. However, in this method, we use the actual calculated isochrone points only for *reference*. The perpendicular distance derived is one taken from linear interpolation between these two points. There is no component taken directly from the isochrone parameterisation, so our probability is entirely reliant on the accuracy of the interpolation.

It is easy to develop contrived examples where linear interpolation produces enormous errors. Consider, for example, the case of a sharp pointed corner in the isochrone where linear interpolation completely cuts off the full extent of the corner, and therefore introduces a large error on any points found near this region.

Of course, with artificial datasets this problem will have no effect whatsoever. The artificial sets are generated using the same linearly interpolated isochrones. It is slightly more worrying therefore that the extent to which this problem affects the results cannot easily be measured. However, several facts suggest that this problem should not be too severe:

(i) Interpolation problems mostly occur around stages of rapid stellar evolution, which are rare. In analysing mainly the RGB we avoid most such loci.

(ii) These stages of rapid evolution are much more carefully analysed in the simulations which produce the isochrones, so the isochrone points are closely spaced at these places. This means that any errors are likely to be kept to a minimum.

(iii) These are not systematic errors, and are distributed in an approximately random fashion on either side of the desired isochrone. The optimisation methods discussed below in section 6 smooth out the occasional anomaly.

Other linear interpolation problems were also considered, such as the problem where the nearest isochrone point to a location in CMD space is at a sharp turning-point in the isochrone. Fortunately testing for this is simple, so methods were developed to correct for the problem.

5.6 Variable photometric errors

As with the treatment of errors in section 2.3, it is necessary here to consider variation of photometric errors over the full spread of colour-magnitude space. Most importantly, the expected value of the photometric error is much larger near the completeness limit as \sqrt{n} and confusion effects begin to have a more considerable impact.

For the Bivariate Gaussian method, the application is rather straightforward. For each point on the isochrone, an associated error in each of the two colours is calculated based on the global error value and the distance from the cutoff in that band.

For the perpendicular distance method, the solution is rather more complicated, and requires calculation of the components of the perpendicular displacement vector in each of the orthogonal directions representing the magnitude and colour. Computationally this is rather slow, but need only be determined once for the assignment of initial probabilities.

6 COEFFICIENT OPTIMISATION

Once the probability matrix, P_{ij} has been generated, the next step is to optimise the coefficients α_j , to maximise the logarithm of the likelihood, as described in equation 12.

This is a constrained maximisation in a space with dimensionality determined by the number of isochrones available. The constraints are;

- (i) The coefficients are constrained to $0 \leq \alpha_j \leq 1 \forall j$
- (ii) The sum of the coefficients is constrained to unity, $\sum_j \alpha_j = 1$

6.1 Background distributions

As already discussed, one encounters problems with anomalous stars in the above method. For stars that lie sufficiently far away from all isochrones to be considered unrelated, numerical problems occur. That is to say, for a star i such that $P_{ij} = 0 \forall j$, one obtains terms from the logarithmic likelihood equation, (12), of logarithms of zero. One way of dealing with this problem is simply to test for zeros and before the logarithm is taken return a very large negative value.

However, a more physically reasonable work around is to introduce a background distribution which attempts to fit all of the anomalous stars and remove them from the problem. This stops the related problem where a star is far from all isochrones except one, and where the weighting for this one isochrone is then increased just simply to enable it to fit this one wayward star.

A sensible assumption in any real dataset is that a certain proportion of the stars are either foreground stars,

background objects such as distant galaxies, or simply spurious. Clearly one does not wish to fit these extra objects and trying to do so would confuse the isochrone weighting algorithms thereby producing incorrect results. A more sensible solution is to just estimate this background fraction, and then introduce a new model, in addition to the isochrones, which essentially represents an isotropic probability density distribution of background objects over all of colour-magnitude space. All stars are guaranteed to fit this distribution, so if we call it model zero, we obtain $P_{i0} = 1 \forall i$.

If we insert this into the equation for the logarithmic likelihood, we then obtain the following analytic form;

$$\log L = \sum_i \log \left(\sigma + \sum_j \alpha_j P_{ij} \right) \quad (19)$$

Here, σ is defined as $\alpha_0 P_{i0}$, which is equal to α_0 independently of i . Therefore, σ is equal to the weighting of the background proportion, and hence affects the degree to which anomalous stars are fitted. This therefore requires slightly different constraints on the normalisation of α if we require the total model weighting to sum to unity. Now we require

$$\sum_j \alpha_j = 1 - \sigma \quad (20)$$

It is worth noting that we fix the value of σ here for one very good reason. Clearly, we could allow the maximisation algorithm to vary the weighting for the background distribution in order to fit it as best it could. However, then it would have freedom to increase the weighting to 1, and reduce all other weightings to zero, because the background distribution is guaranteed to fit all stars, by definition.

One could equally well introduce a functional form for the background distribution where it varied depending on the magnitude or colour of the stars it was fitting. In that case it would be necessary to precalculate the values of P_{i0} , which would now no longer all be equal to unity, but would vary with i . This method would be useful for fitting background stars in fields which are known to be contaminated with, for example, faint blue background galaxies, or perhaps a foreground star cluster, and where reliable offset data are available. Another interesting possibility would be to simulate the background distribution for fields close to the Galactic disk, using a simple galactic model.

6.2 Smoothness constraints

As suggested earlier in section (5), it is possible to introduce any prior information about a particular field, or the functions under consideration, in order to restrict the range of the fit. One further consideration is the smoothness of the metallicity function. This can be a desirable property.

For example, we might not expect spiky metallicity distributions, but rather a much smoother shape, or vice versa. Introducing these constraints into the likelihood function allows us to optimise the fitting procedure in either situation.

The implementation is numerical rather than analytic. We introduced code into the likelihood calculation function that penalises large steps in α and also reduces the likelihood depending on the number of individual maxima in

the metallicity distribution, hence selecting against particularly rough distributions. In complex stellar populations, one expects a certain degree of roughness e.g. caused by late accretion events. Smoothing levels must be tested to ensure that the metallicity distributions returned are not losing real information.

A second method is to estimate the expected uncertainty in the metallicity values obtained, and to convolve a Gaussian of this width with the final metallicity distribution. Our second paper will deal in more detail with the estimation of intrinsic errors due to distance and age uncertainties.

7 MAXIMISATION ALGORITHMS IN MULTI-DIMENSIONAL PARAMETER SPACE

We have now developed a method for calculating the degree to which any distribution is fitted by a given linear combination of isochrones, parameterised by coefficients α_i . All that remains is to optimise these coefficients using some algorithm to be determined.

The sections are labelled in order of increasing complication, with the latter methods being both more difficult to fine-tune, but also more successful when working correctly.

As a first guess, it is accurate enough simply to analyse the probability matrix, and build up a normalised set of coefficients based on how many stars each isochrone fits best. One loops through each star, and calculates which isochrone has the highest probability of producing this star, that is to say find the value j for a star i which maximises P_{ij} . A tally of how many stars are best fit by each isochrone is made. Once all stars have been considered, we normalise the tally vector and set this as the initial coefficient vector.

Clearly this is a good first guess, but there are problems with this method. Most obviously, in places where the isochrones are crowded, it is quite possible that a star will be best fit by an isochrone which is not the correct isochrone, and is not even adjacent in metallicity. This problem is enormously reduced by using the perpendicular distance method as discussed above.

7.1 The Gradient Walker Algorithm

To visualise the problem, it will prove useful to imagine the simplified case of maximising a function of two variables, and then simply to extend this mathematically to a larger number. One can readily imagine a height field where the height $h(x, y)$ is a function of the two orthogonal cartesian displacements x and y . The problem is to find the maximum value of the function h given the constraints that $x \geq 0$ and $y \geq 0$ and also that $x + y = 1$. If we forget about the third of these constraints for a moment, we can imagine the problem as maximising the function h over a region of the x, y plane.

In many dimensions, we can generalise this problem to that of maximising a function of n variables with $n + 1$ constraints. Namely, that each of the separate variables must be positive, and that the coefficient vector, α is constrained to lie within the hypersurface defined by $\sum_j \alpha_j = \text{constant}$.

The most obvious method of finding the maximum of this function is a so-called *gradient walker*. That is to say,

one takes a series of steps where at each point the gradient of the function is evaluated, and then some scalar multiple of this vector is added to the coefficient vector. The coefficient vector is then renormalised and the new likelihood is calculated. This method is repeated until a maximum is found.

7.1.1 Calculating the gradient

One can in principle calculate the gradient of the likelihood function easily. The following is the appropriate formula to use;

$$\frac{\partial \log(L)}{\partial \alpha_k} = \frac{\log(L(\alpha + \epsilon_k)) - \log(L(\alpha))}{\epsilon} \quad (21)$$

where ϵ_k is some small incremental vector equal to the following;

$$(\epsilon_k)_j = \begin{cases} \epsilon & \text{if } j = k \\ 0 & \text{if } j \neq k \end{cases} \quad (22)$$

This calculation has to be performed for every dimension, essentially once per isochrone. When there are several hundred, or even thousands of isochrones to fit then this method becomes costly. However, the expectation is that this calculation need only be performed a few times before the maximum is reached.

7.1.2 Variable step length

Assuming the gradient vector can be calculated, it is then normalised to unit length and multiplied by a scale factor depending on how much we wish to alter the coefficients. This value is very much open to fine-tuning, and it is principally a matter of experimentation to discover the optimum in any specific application.

Of course, the gradient step can, and should be altered depending on how close one estimates one is to the maximum of the likelihood function. This can be approximated by the following method, using the data from the last step taken;

$$\text{Improvement} = \frac{\text{Increase in } \log(\text{Likelihood})}{\text{Previous Step Length}} \quad (23)$$

One then examines the *Improvement* score, and alters the length of the gradient step accordingly. If we are near the maximum then we would expect the *Improvement* score to be rather low, indicating that it is difficult to improve the likelihood by an appreciable amount. However, if we are nowhere near the maximum then we might expect the value of the *Improvement* to be rather larger, indicating that it is fairly easy to improve the likelihood and that a longer step length should be taken.

Of course this method is all rather approximate. What we require is a more exact algorithm which generates the optimum step lengths at a given position. That is what the conjugate gradient method describes.

7.2 Conjugate gradient method

The conjugate gradient method is a refinement of the variable step length algorithm of section 7.1.2. After one has calculated a normalised gradient vector then add on a scalar

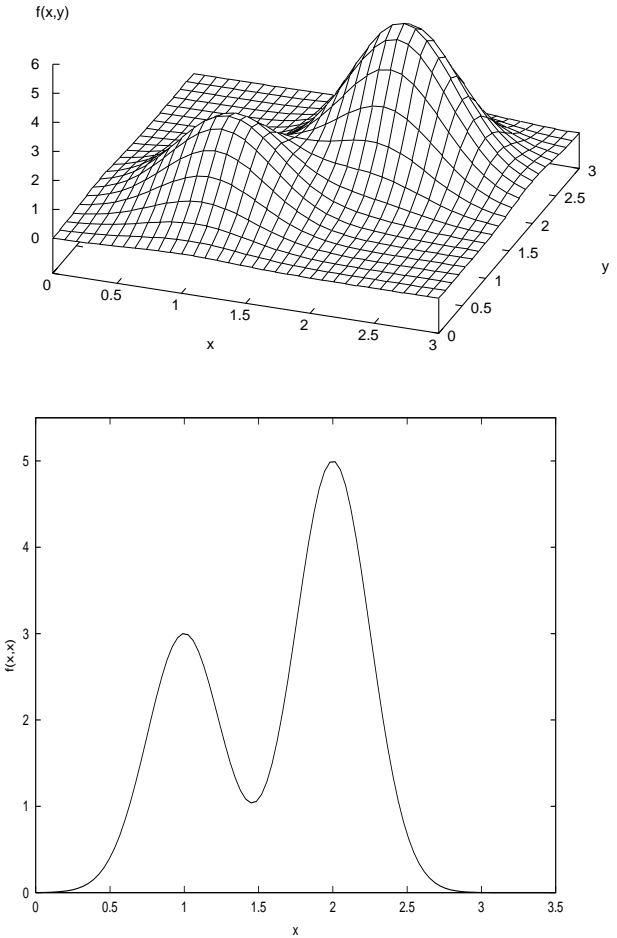


Figure 6. Two Gaussian peaks in the (x,y) plane. One is located at $(1,1)$ with magnitude 3 units. The larger is located at $(2,2)$ with magnitude 5 units. Underneath is a cross-section along the line $y = x$.

multiple of this vector to the current coefficient vector such that the likelihood is maximised under the given constraints. That is to say, we wish to find a value of λ which maximises the following quantity, Ψ ;

$$\Psi = L(\alpha + \lambda \nabla L) \quad (24)$$

This method means that the gradient step size is always optimal, and that therefore we reach the maximum most quickly. Notice that we are not sure that this is the *global* maximum, and therein lies the failing of this method, and indeed the variable step length method. It is often rather straightforward to find a *local* maximum of the likelihood function, but ensuring that this is a *global* maximum requires more consideration. However, this method is an improvement on the method outlined in section 7.1.2, as the following hypothetical illustration demonstrates.

Consider we are maximising a function f of two variables, x and y , over the positive domain. This function f has two local maxima at $(1, 1)$ and $(2, 2)$. The latter is a slightly larger maximum, and is therefore the global maximum. The maximisation procedure starts at the origin. This situation is illustrated in figure (6).

Using the gradient walker technique, it is easy to see that the actual maximum found depends to a large extent on the choice of gradient steps. If the gradient step takes the current coordinates nearer to the slightly smaller peak then the chances are that will be the one that is found to be the maximum. It is clear that a short step length will preferentially climb the nearer peak first, eventually reaching the local maximum without even considering the second, slightly larger but more distant maximum.

However, with a long step length, one can envisage a situation where both peaks are ‘overshot’. One could even end up with an oscillatory set of solutions in turn overshooting in the positive direction, then overshooting back in the negative direction.

It is clear that the variable step length method has many serious problems, which are solved by using the conjugate gradient method. In this example, the conjugate gradient method would immediately find the global maximum from the initial position, as the gradient is in the direction $(1, 1)$, which passes through both peaks.

However, one could imagine a more likely situation where the second, larger peak does not lie on the same line as the smaller peak. Imagine the above situation with the second peak displaced from $(2, 2)$ to $(3, 2)$, but with the same magnitude as in figure 6. This situation is shown in figure 7. The gradient at the origin would still point approximately towards the peak at $(1, 1)$, but would miss the larger peak completely. Even the conjugate gradient method would fail here, and return the smaller local maximum instead of the larger, global maximum.

A new algorithm is required which is more efficient at finding global maxima, and furthermore deals more effectively with larger dimensionality. An algorithm ideal for such an application is ‘simulated annealing’.

7.3 Simulated Annealing

The method of simulated annealing draws from the realm of materials science, but only in concept (Kirkpatrick, Gelatt & Vecchi, 1983a). It is designed to simulate stochastically the cooling of a physical system in a sufficiently general sense for it to be applicable to many other optimisation problems where the global minimum or maximum of a function is required.

Simulated annealing requires three components. Firstly, a cost function, related loosely to the Hamiltonian in a real physical system. This is the function which is to be extremised, in this case the logarithmic likelihood function of the coefficients, α . Secondly, we require some method of generating random steps within the constrained region in which the cost function is to be extremised. Finally, some ‘temperature’ must be defined, which affects the degree to which random steps are accepted based on the variation of the cost function. This temperature obviously corresponds to no real quantity, it is simply a device used for algorithmic purposes.

This ‘temperature’ parameter is decreased over time either linearly, or in some more complicated manner, see section 7.3.2. Random steps are generated, and are accepted depending on the value of the Hamiltonian or cost function at the new point relative to the previous point. In most cases, this cost function is to be minimised, but with our problem the cost function is the logarithmic likelihood function,

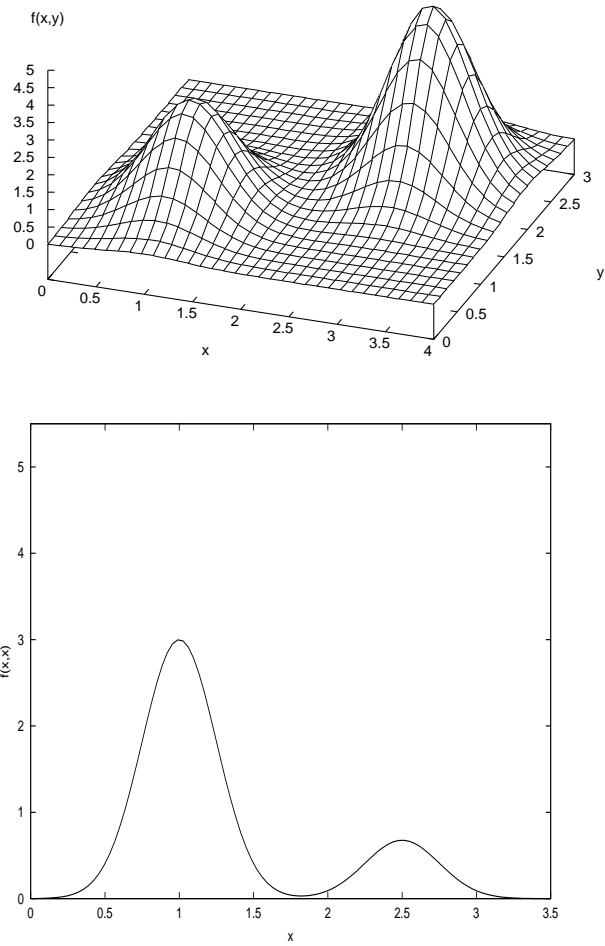


Figure 7. In this diagram, the larger peak of magnitude 5 units has been moved to position $(3, 2)$. c.f. figure 6. Underneath is a cross section along the line $y = x$.

which we wish to be maximised. Any step which increases the likelihood is automatically accepted. Furthermore, any step which decreases the likelihood is accepted with a certain probability given by;

$$P(\text{step}) = \exp\left(\frac{\Delta \log(L)}{T}\right) \quad (25)$$

Here, T is the ‘temperature’ value described above. For all $\Delta L < 0$, this acceptance probability is less than unity. The larger the drop in the likelihood, the smaller the chances of accepting the step. However, at higher temperatures, ‘backward’ steps are more likely. This stops the optimisation from rapidly centering on the nearest local maximum without considering the global situation. Clearly, if a large maximum is found at any point then the chances of leaving it are smaller because most steps will lead to significant drops in the likelihood.

As the temperature drops closer to zero, detrimental steps become increasingly less likely, and the optimisation algorithm begins to centre on the current maximum, which is expected to be the global maximum.

Clearly some care needs to be taken in the correct implementation of this algorithm as there are so many different

values to fine-tune. The main two areas where some thought is required are in the generation of random steps, and in the temperature decrement function.

7.3.1 Choosing random steps

Clearly, with a dimensionality of several hundred, it is important that a sensible random step is chosen such that the probability of moving in a useful direction is maximised. However, one cannot simply bias the step significantly by the local gradient as this would then remove the advantages of this method in avoiding local maxima which were not the largest globally.

After some experimentation, we discovered that the most efficient way of altering the coefficients was to perturb each of the coefficients by a value proportional to the coefficient itself, at the 10 percent level. That is to say that for each coefficient, α_i , the perturbation obeyed $-0.1\alpha_i < \delta_i < 0.1\alpha_i$.

One further optimisation which could be performed on the step generation algorithm is simply to add some small percentage of the current local gradient on to the step to bias the solution towards high likelihood areas. An analogy of the simulated annealing method is to imagine a ball bouncing across a 2D surface, where at each point a small percentage of its internal energy is lost. In the minimisation algorithm, we require that the ball eventually finds itself in the deepest minimum in the range of the variables. In our scheme, we require the maxima to be found, but the concept of balls falling into holes is much more straightforward to visualise, and the algorithm is absolutely identical except for a sign change.

In the above example, we can cause the ‘ball’ to jump preferentially towards the areas we are interested in by adding on a small fraction of the local gradient. Considering a minimisation problem, that effectively means that the ball will preferentially bounce downhill, as one would expect. One modification to the step generation algorithm therefore would be to add on a certain fraction, β , of the local gradient, where β is a function of the system temperature, T . That is to say that at high temperature the ‘bouncing’ is largely random, whereas as the temperature falls it becomes increasingly biased towards moving towards the minimum points. Again, this requires considerable fine-tuning.

For our work, we considered a simple inverse function to generate the dependence of β on the temperature, T . That is, $\beta \propto \frac{1}{T}$. As T decreases, the fraction of the gradient added on increases towards very large values. In theory we encounter problems as T tends towards zero, but in practice we truncate the search before T actually reaches zero, so these floating point errors are avoided.

In order to maintain the normalisation constraints on the gradient step, that is to say the total step length remaining roughly constant over time, the true form of the perturbations becomes the following:

$$\alpha_i \Rightarrow \alpha_i \left(1 + \frac{\beta \nabla_i \log(L) + R[-1, 1]}{10(\beta + 1)} \right) \quad (26)$$

This assumes that the gradient is normalised to unit length. In this notation, $R[-1, 1]$ represents a random number uniformly distributed in the range -1 to +1.

Now that we have established a realistic step generation

function, it is necessary to determine the way in which the temperature decreases over time, as well as the initial value of the temperature.

7.3.2 Temperature decrement function

In this work we consider only simple temperature decrements of the form $T \Rightarrow aT - b$. That is to say a geometric part and an arithmetic part. a and b are free parameters here, as is the initial value of the temperature, T_0 .

There are no hard-and-fast rules for determining these quantities, so they were all varied until an optimal value appropriate to the implementation at hand was discovered. Varying the value of T_0 alters the amount to which random steps are important near the beginning of the optimisation procedure. The larger the value of T_0 , the more likely the particle is initially to take a totally random step to a position of lower likelihood. Whereas this is rather useful if one does not have a good initial guess of the global maximum, this is not the case here. We can efficiently start with a reasonably low value of T_0 , and then alter it slightly depending on the values of a and b and the total number of steps required.

As for the values of a and b , a little more experimentation was required. We initially attempted to find optimal solutions with either one removed in turn. Firstly, with $a = 1$ and $b > 0$, that is a purely linear decrease in T , we found that the solutions were not optimal for several reasons. Most importantly, the majority of the optimisation happens at low T when the method simply requires to centre in on the final maximum point. With a linear decrease, the time spent at low temperature is exactly the same as the time spent at high temperature for a unit temperature interval. That means that there is no bias towards locating an accurate maximum against randomly wandering about parameter space.

However, if we set b to zero and we are left with a purely geometric decrement function, then we spend far too long at low temperatures. Indeed, a low- T cutoff must be introduced in order to prevent the search continuing for ever. The benefits in spending so much time at low temperature are unclear, and probably negligible. By experimenting with the value of a between 0.95 and 1.00, it was possible to test a reasonable segment of parameter space in order to test the time it took for a maximum to be found.

We combined the two parameters together on an example dataset, a single delta function population at 10Gyr and $[Fe/H] = -1.0$. In table (1) we list the number of steps required and the final maximum likelihood obtained for different combinations of a and b using a value for the initial ‘temperature’ of $T_0 = 8$. Values of a run across the top and $b * 10^4$ down the left hand side. For testing purposes, a uniform distribution was chosen as a first guess in all cases.

Note that the logarithmic probability values are often greater than zero. As previously stated, these are only *relative* values so the absolute values are not important, just their differences. Of course, there is also a certain amount of random variability in this too, but repeated tests on a few of the settings showed that it was no greater than ± 0.2 in the maximum likelihood for those close to the seemingly maximal value, and usually much less. For those coefficients which didn’t get near to this value then the variation was

a=	0.995	0.996	0.997	0.998	0.999	1
$b * 10^4 =$	0	211.1/1793	211.5/2243	211.5/2992	211.7/4490	211.6/8993
	1	162.3/1187	205.5/1431	211.0/1816	211.4/2529	211.4/4383
	2	-176.7/1054	158.6/1263	209.9/1592	211.2/2191	211.2/3707
	3	-360.4/975	17.4/1165	207.6/1460	210.9/1993	211.1/3316
	4	-426.2/919	-91.0/1094	202.7/1366	210.9/1853	211.1/3041
	5	-480.3/875	-226.5/1040	200.0/1294	210.4/1745	211.1/2830

Table 1. The effect of changing the values of the coefficients a and b in equation $T \Rightarrow aT - b$. Values given are final likelihood/ number of steps required. Optimal values seem to be around a balanced medium of these two parameters, such as $a = 0.998$, $b = 0.0002$.

significantly more, but never brought the likelihood high enough to be worth considering.

Clearly, it is important to spend some time at low temperature values optimising the coefficients towards a local maximum. This is shown by the clear trend in likelihood with increasing a . However, the number of steps also increases with increasing a , so a balance must be found.

7.4 First-guess isochrone coefficients

The initial guess for the isochrone coefficients is calculated by considering the number of stars which are best fit by each isochrone. The expectation is that a good first guess will prevent the optimisation procedure from falling into incorrect local maxima of the probability function instead of the global maximum. The likelihood calculation should also proceed more quickly if many of the original coefficients can also be ignored right from the start, as this would allow us to sum over fewer variables.

However, this method introduces several important dangers. Firstly, one must always exercise caution when adding prior data to any such optimisation problem. If the prior knowledge is either inaccurate or simply misleading then there is a possibility that it might bias the output of the test. Secondly, it is important to test that the general form of the recovered metallicity distribution is not actually a strong function of the chosen first-guess coefficient distribution.

To test these results, we generated an artificial dataset composed of 500 stars generated from a triple input population of thin metallicity spikes at metallicity values of $[Fe/H] = -1.0, -0.8$ and -0.6 . We then carried out the optimisation procedure using the best first-guess coefficients to test the recovery quality. We also tested the recovery using a flat first-guess with all coefficients set to the same value. Thirdly, we tested using completely random initial coefficients using a standard random number generator with an unbiased, flat probability distribution.

Plotted in figure 8 are the recovered metallicity distributions for the above populations. There are six distributions plotted, and it is clear that none of these differs from the original recovered distribution by more than a small amount. This is reassuring, and demonstrates that the recovered metallicity distribution is not a strong function of the input distribution, though the assumption of a realistic first-guess coefficient distribution does slightly improve the overall fit.

Rather encouragingly, the third metallicity spike appears double in the diagram, with the first-coefficient guess

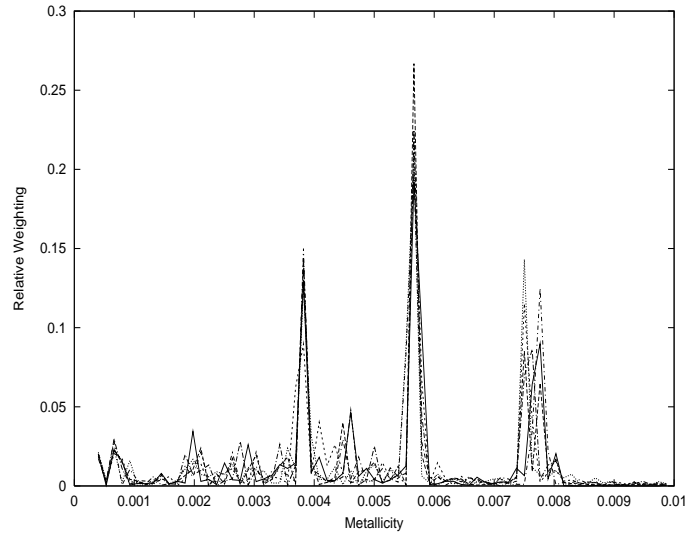


Figure 8. Testing the results gained as a function of the initial coefficient distribution using a best-guess coefficient set (solid line), a flat distribution (dot-dashed line) and completely random metallicity distributions (other lines). Clearly the initial coefficient distribution does not bias the output strongly.

slightly biasing the output result. However, the adopted method, that is the method where the initial coefficients are assigned best-guess values, produces by far the most accurate fit to this third population. In general, the form of the fitting curves is unchanged regardless of initial coefficient distribution.

All three central values seem to be slightly underestimated in this particular test. This is an interesting artefact of the photometric errors. Broadening the narrow-abundance populations using Poisson errors meant that stars were spread out over a wider metallicity range. In this situation, our code will tend to underestimate the metallicity value because the isochrones towards lower metallicity are more closely packed. This means that a slight reduction in the peak metallicity value will fit a larger number of isochrones more accurately. Ideally we should try to space the isochrones evenly in colour-magnitude separation rather than in metallicity, but this is not possible in practice because the isochrones are not parallel.

7.5 Monte-Carlo enhancements

One way to solve this problem is to introduce the idea of Monte-Carlo steps after the temperature drops to a certain

low threshold. In a sense, this means continuing the simulated annealing algorithm, but with a zero temperature. Random steps are taken and accepted only if they improve the likelihood. In the previous analogy, it is like allowing the “ball” to roll down the “holes” towards an optimum value.

To implement this method, we used similar routines to the simulated annealing approach. Firstly, a subset of the coefficients were selected, and then perturbed by a certain random percentage, as above. A new likelihood was then calculated, and if it was an improvement then the step was taken. If it was not an improvement then the new coefficients were rejected.

This algorithm was continued until a certain number of quiescent perturbations had been performed. We defined “quiescent” as perturbations which did not improve the likelihood above a certain small value. This stopped the Monte-Carlo optimisation routine from continuing ad infinitum with infinitesimally small improvements which had no real effect on the overall metallicity distribution recovered.

We also used a slightly smaller step length in this algorithm, as we were expecting the coefficients to already be reasonably near the global maximum, so only small perturbations were required. Clearly we require a reasonably accurate guess to the maximum from the annealing method or the Monte-Carlo steps could potentially continue for an unreasonably long time.

In addition, after every perturbation step the coefficients perturbed were recorded, together with the direction in which they were perturbed. If a perturbation improved the likelihood then the same coefficients were reconsidered with the same perturbation directions. This continued until the likelihood no longer improved.

This method allows a much more accurate determination of the true maximum point to be established. The overall effect was never to truly change the metallicity distribution, so this method was only used when the most accurate answer possible was required. Clearly there is a certain level after which this kind of further optimisation is irrelevant. The errors inherent in the optimisation procedure itself together with the method of assigning initial probabilities have a far greater effect. However, the method is certainly generally applicable to problems where greater accuracy is both possible, and required.

In figures 9 and 10 we demonstrate a small selection of results generated by the metallicity distribution fitting programme, *FITCOEVAL*. We have tested this programme on the artificial datasets generated by the code described above. Diagram captions explain in greater detail the fitting methods employed.

8 CONCLUSION

We have presented appropriate tools and methods for generating and analysing colour magnitude diagrams for old giant-branch stellar populations. Our subsequent work has allowed us to test the accuracy of these methods, and to develop new algorithms to introduce Bayesian prior knowledge into the fitting procedure.

Using the tools outlined in this paper we can now do the following:

- (i) Create artificial colour-magnitude diagrams, paying

attention to the many different sources of error inherent in conventional observational techniques.

(ii) Compare artificial colour magnitude diagrams to those obtained from observations using any of a number of methods, including that outlined by Harris & Zaritsky (2001).

(iii) Fit a maximum likelihood metallicity distribution to old RGB stellar populations using an interpolated grid of theoretical isochrones.

The second paper of this series (to be published soon) discusses the limitations and systematic errors involved in RGB isochrone fitting methods. We treat the handling of errors both in the computational methods employed, and also in the isochrone models themselves. We derive limits to which isochrone fitting can help us to obtain information about the RGB populations of nearby galaxies.

9 ACKNOWLEDGMENTS

C.M.F. would like to extend his thanks to Jan Kleyna for help in the preparation of the code required for this project, and also to Richard de Grijs for many interesting discussions on these topics and valuable comments on early drafts of the paper.

REFERENCES

Aparicio A. et al., 1996, ApJL, 469, L97
 Ashman K.M., Zepf S.E., 1992, ApJ, 181, 4301
 Baugh C.M., Cole S., Frenk C.S., 1996, MNRAS, 283, 1361
 Baugh C.M. Cole S., Frenk C.S., Lacey C.G., 1998, ApJ, 498, 504
 Bertelli G., Betto R., Chiosi C., Bressan A., Nasi E., 1990, A&AS, 85, 845
 Bruzual G., 1983, ApJ, 273, 105
 Bruzual G., Charlot S., 1993, ApJ, 405, 538
 Charlot S., Bruzual G., 1991, ApJ, 367, 126
 Daddi E., Cimatti A., Renzini A., 2000, A&A, 362, 45
 Dolphin A., 1997, New Astronomy, 2, 397
 Girardi L., Bressan A., Bertelli G., Chiosi C., 2000, A&AS, 141, 371
 Harris J., Zaritsky D., 2001, ApJS, 136, 25
 Hernandez X., Valls-Gabaud D., Gilmore G.F., 1999, MNRAS, 304, 705
 Kauffmann G., 1996, MNRAS, 281, 487
 Kirkpatrick S., Gelatt C.D., Vecchi M., 1983, Science, 220, 671
 Kroupa P., Tout C.A., Gilmore G.F., 1993, MNRAS, 262, 545
 Salaris M., Chieffi A., Straniero O., 1993, ApJ, 414, 580
 Tolstoy E., Saha A., 1996, ApJ, 462, 672
 Whitmore B.C., Schweizer F., 1995, AJ, 109, 160
 Whitmore B.C., Zhang Q., Leitherer C., Fall S.M., Schweizer F., Miller B.W., 1999, AJ, 118, 1551

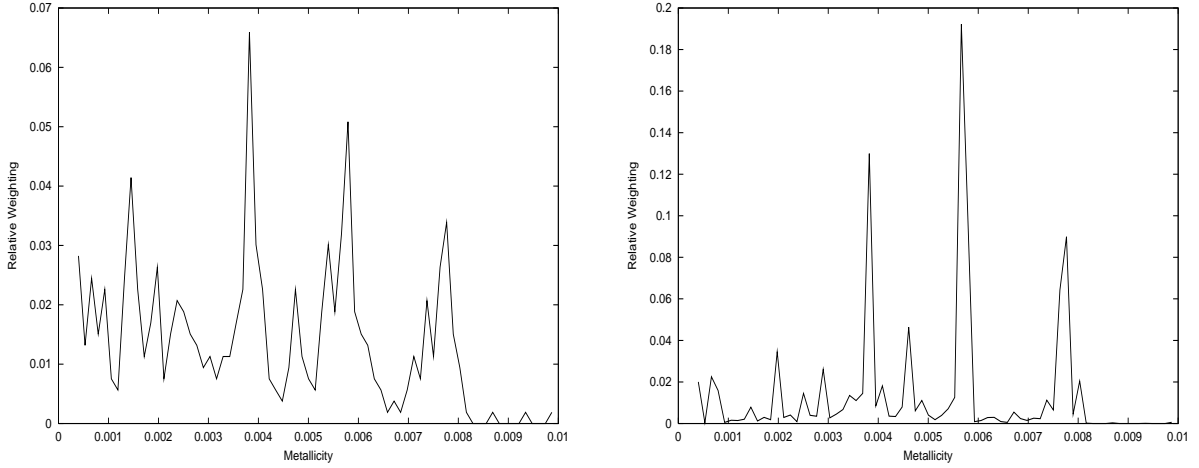


Figure 9. Left: The first guess coefficient values for the sum of three equal size delta populations at metallicities of $[Fe/H] = -1.0, -0.8$ and -0.6 . Poisson errors and 3 per cent photometric errors were introduced into the simulated dataset. Right: The final optimised version after simulated annealing and Monte-Carlo optimisations. Residual errors are caused by the Horizontal Branch, which is notoriously difficult to fit. By fitting only the RGB, the quality of fit is significantly improved. See the next paper in this series for a more rigorous investigation.

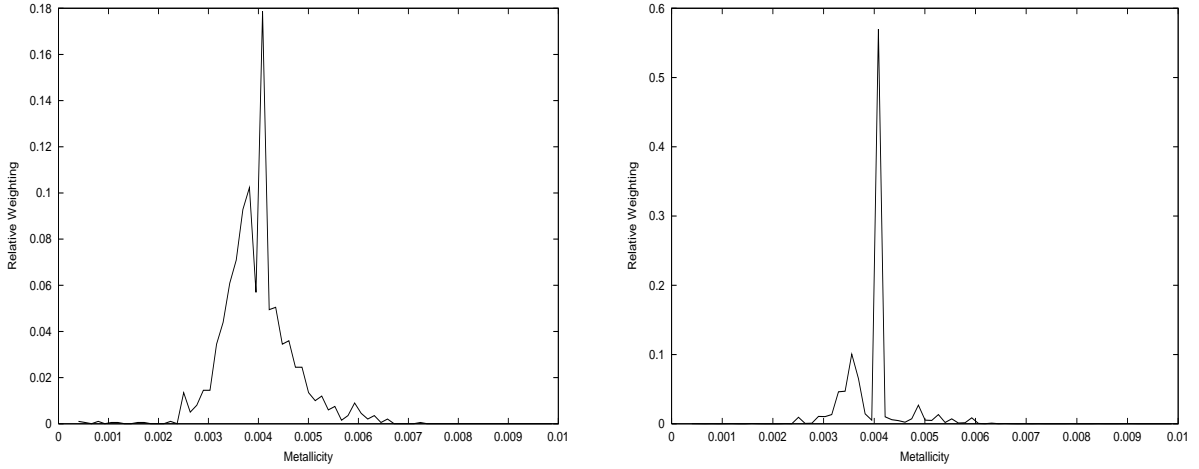


Figure 10. Calculated best fit coefficient values for a non-coeval population centred on 10Gyr and a metallicity of $[Fe/H] = -1.0$. We added a narrow age spread of ± 0.3 Gyr into the initial data in order to test the degree to which this affected the recovery of the central metallicity value. Poisson errors and 3 per cent photometric errors were introduced into the simulated CMD. Left: First guess before optimisation. Right: The final version after simulated annealing and Monte-Carlo optimisations.